A98-31527

ICAS-98-2,10,2

LARGE-EDDY SIMULATION OF A TRAILING VORTEX SYSTEM BEHIND A CIVIL AIRCRAFT MODEL

C.B. da Silva, J.M.M. Sousa and J.C.F. Pereira

Instituto Superior Técnico/Technical University of Lisbon
Mechanical Engineering Department
Av. Rovisco Pais, 1
P-1096 Lisboa Codex, Portugal

Abstract

In this paper we investigate Flap-Tip vortex pair interaction behind a civil aircraft model. We perform Large-Eddy Simulation of a pair of Burgers vortices, whose parameters were set according to wind tunnel measurements of a Flap-Tip vortex pair issuing from a civil aircraft model. The study of the isolated (Flap) vortex provides us significant insight about its turbulent structure. In the Flap-Tip vortex system we see how the interaction of the vortices modifies their mean and turbulent flow fields. The work ends with the study of the effect of initial separation distance on the vortex pair development.

Introduction

It is well known that strong, concentrated ribbon-like vortices develop in the trailing wake of an aircraft, resulting from the presence of lifting surfaces. On the other hand, it is also recognized that hazardous scenarios stemming from wake-vortex encounters are especially worrisome during "take-off" and "landing approach", when the separation distance between individual aircrafts is relatively small. Still in addition, Tip vortex circulation has shown to be maximal when a plane is near the runway, while the deployment of high-lift configurations during the aforementioned flight segments originates the formation of rather complex flow topologies in the trailing vortex system. [1-2] The awareness that the influence of the near-field characteristics on the far-field of the wake is poorly understood has set an urgency to investigate this issue, leading to a number of wind-tunnel campaigns. However, regardless of the capital importance of the availability of reliable experimental data describing the wake vortices trailing in the vicinity of an aircraft, thorough characterisations of the associated flow field along the freestream direction constitute very expensive efforts. Further, even if the plane is scaled down by a significant ratio to the actual size, most test facilities restrain the flow survey to distances not much larger than one wing span. Thus, the application of modern numerical techniques, which may prove to cope with the necessary requirements to produce both realistic and accurate simulations allowing the extension of wind-tunnel data, is highly desirable.

In the present study, the development and interaction of a Flap-Tip vortex system in the near-wake field behind a civil aircraft model has been investigated by Large-Eddy Simulation (LES). We emphasise that we are mainly interested in using LES as an engineering tool, to understand the physics of Flap-Tip vortex interaction in the near-wake, in addition to catching the most important parameters of the flow and their interplay during the roll-up process.

First we have focused on the development of a single (Flap) vortex. The absence of a substantial degree of meandering enabled us to properly study the evolution of the mean flow field and turbulent stresses. With the light cast by this study, we analysed the Flap-Tip vortex interaction. Particular emphasis was given to the investigation of the following issues: how the Flap vortex "feels" the presence of the Tip vortex (orbiting around it); and to which extent the presence of the Tip vortex modifies mean and turbulent fields characterising the Flap vortex. Finally, we investigated the influence of the initial Flap-Tip vortex separation distance on its downstream evolution.

Flow Model

Governing Equations, Numerical Model and Subgrid-Scale Modelling

The development of the trailing vortex system has been numerically simulated by solving the three-dimensional, unsteady, filtered Navier-Stokes equations:

$$\frac{\partial \tilde{u}_i}{\partial x_i} = 0 \qquad (1)$$

$$\frac{\partial \tilde{u}_i}{\partial t}+\frac{\partial}{\partial x_j}\left(\tilde{u}_i\tilde{u}_j\right)=-\frac{1}{\rho}\frac{\partial \tilde{p}}{\partial x_i}+\frac{\partial}{\partial x_j}\left\{\nu\left(\frac{\partial \tilde{u}_i}{\partial x_j}+\frac{\partial \tilde{u}_j}{\partial x_i}\right)+\tau_{ij}\right\}. \qquad (2)$$

Here, ν is the cinematic eddy viscosity, ρ is the density and $\tilde{u}_i(\mathbf{x},t)$ is the spatially filtered velocity field, obtained by convolving the original velocity field with a filter function $G(\boldsymbol{x},\boldsymbol{x}')$ over the entire domain D:

$$\tilde{u}_i(\mathbf{x},t)=\int_D u_i(\mathbf{x}',t)G(\mathbf{x},\mathbf{x}')d\mathbf{x}'. \qquad (3)$$

The subgrid-scale stresses (SGS): $\tau_{ij}=\tilde{u}_i\tilde{u}_j-\tilde{u_i u_j}$ describe the influence of subgrid scales on large resolved scales of the flow and it must be modelled. For that purpose, we used Smagorisky's model. As in the majority of models, it makes use of an eddy viscosity assumption (Boussinesq´s Hypothesis),

$$\tau_{ij}-\frac{\delta_{ij}}{3}\tau_{kk}=2\nu_t\tilde{S}_{ij}, \qquad (4)$$

where ν_t is the eddy viscosity and $\tilde{S}_{ij}$ is the filtered rate of strain rate tensor,

$$\tilde{S}_{ij}=\frac{1}{2}\left(\frac{\partial \tilde{u}_i}{\partial x_j}+\frac{\partial \tilde{u}_j}{\partial x_i}\right). \qquad (5)$$

The eddy viscosity is then given by

$$\nu_t=(C_s\Delta)^2\left|\tilde{S}\right|, \qquad (6)$$

with $\left|\tilde{S}\right|=\left(2S_{ij}S_{ij}\right)^{1/2}$. Finally, C_s stands for the Smagorinsky's constant, which we set equal to 0.10, and Δ is the spatial filter width (usually computed as $(\Delta x\Delta y\Delta z)^{1/3}$ in anisotropic grids).

Concerning the numerical method, the filtered Navier-Stokes equations have been discretized using the finite-volume method over an orthogonal, staggered grid system. Discretization was accomplished using an explicit quadratic Leith-type of temporal discretization. Full details can be found in Pereira and Sousa. [3-4]

The computational domain was constructed with roughly 1.4 (m) in streamwise direction and 2.8 (m) in the remaining orthogonal directions (in the plane of vortex cores). Higher resolution was placed in the region overlapping the vortex cores to account for the larger gradients occurring in this area. Consequently, at least 8 points were used to describe the diameter of each vortex core. The total number of points was approximately 1/2 million mesh points.

The boundary conditions used were the following. As inlet condition, we prescribed our vortex models (described below) adjusted to Huenecke's [5] measurements. Non-reflective boundary conditions were implemented at lateral and outlet boundaries. With the use of these boundary conditions we expect to obtain much more realistic results than those yielded by classical von Newmann boundary treatment.

A preliminary study had to be carried out in order to determine the most realistic way of disturbing the inlet flow fields. Because we wanted to simulate as accurately as possible an already fully turbulent flow field, we did not wanted to impose an initial perturbation that would make the code to react abruptly, adjusting itself to an unphysical inlet profile. Our main goal was to provide an initial perturbation that allowed the flow to evolve smoothly from the inlet of the domain. Thus, the initial perturbation was designed in such way that consistency with the SGS model would be kept. As a result, the initial fluctuations (for each velocity component) were based on Gaussian noise superimposed to normal stress components computed by Smagorisky's model.

Vortex model

The computations were started at an assumed distance (from the trailing edge of the wing) of about two and a half wing chords. At such stage, the roll-up process of both (outboard) Flap and Tip vortices is expected to exhibit a reasonable degree of maturation. Extensive experimental measurements have shown that the circunferential velocity profile associated to the vortex is well represented by a two-dimensional Burgers vortex. [6] Thus, based on the above mentioned assumptions, the complete velocity flow field imposed as inlet boundary condition to the computational domain was obtained by superimposing a pair of staggered Burgers-type vortices. Tangential and axial velocity profiles for each one of the vortices (Flap and Tip) were specified by

$$v_\theta=\left(\Gamma_o/2\pi r\right)\left\{1-\exp\left(-ar^2\right)\right\}, \qquad (7)$$

$$u=U_\infty-\Delta U_o\exp\left(-ar^2\right). \qquad (8)$$

Here, Γ_o is the initial circulation, U_∞ is the freestream velocity ($U_\infty=60$ ms^{-1}), ΔU_o is an axial

velocity deficit occurring at the vortex centreline and a is a constant related to the vortex core diameter r_o. Realistic values for the parameters have been used on (7) and (8), aiming to approximate the flow conditions for a 1:16 model of a medium-range, twin-engined civil aircraft at high-lift configuration [5]. The values used are given in Table 1.

Vortex	Flap	Tip
Γ_o (m^2s^{-1})	1.249	0.705
r_o (m)	0.0325	0.025
ΔU_o (ms^{-1})	0.2 U_∞	0.183 U_∞

TABLE 1 – Initial parameters for Flap and Tip vortices (from Huenecke [5]).

Single Vortex

We begin this investigation with the study of an isolated (Flap) vortex. The mean flow development can be seen through Figures 1 to 4. In Figures 1 and 2 one may see tangential and axial mean field velocities at Station 31 of the computational mesh, corresponding to a distance X = 0.469 (m) from the inlet domain boundary. The streamwise development of a single vortex is shown in Figures 3 and 4. Concerning these mean fields one may perceive, as expected, a very slow radial diffusion of tangential momentum that increases the vortex core radius and decreases its tangential velocity, as the vortex is carried away by the mean axial velocity field.

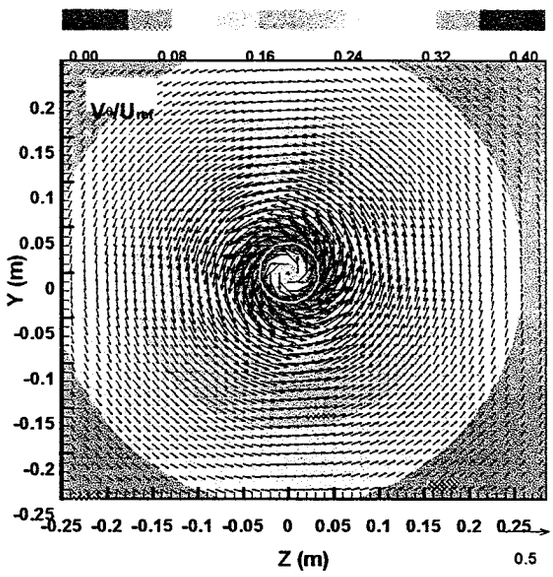

FIGURE 1 – Tangential mean velocity map at Station 31, X = 0.469 (m). The white circle marks the initial (inlet) location of the vortex core.

If one computes the time spent by the vortex to travel over the computational domain (relating the convective axial velocity with the distance travelled by the vortex) one may compare the rate of decay of the calculated tangential velocity with that predicted by theory, for a Lamb-Oseen vortex. It seemed that this rate of tangential velocity decay, being mainly dictated by radial velocity gradients, should be equal to that of a Lamb-Oseen vortex. However, we observed that the present rate of tangential velocity decrease is slightly larger than that of a Lamb-Oseen vortex. One must point out that, in these calculations, we are dealing with a spatial simulation where three-dimensional effects (namely, production of vorticity) may lead us to a totally different physical situation. Furthermore, in a turbulent vortex, radial diffusion of vorticity is mainly dominated by turbulent viscosity, as shown by Zeman. [7] The corresponding viscosity coefficient can be significantly high in LES performed on a rather coarse grid, as in this case. This may well be one of the reasons why some of the measured trailing vortices systems exhibit a tangential velocity decay differing from that predicted by the Lamb-Oseen model (see, e.g., Spalart [8]).

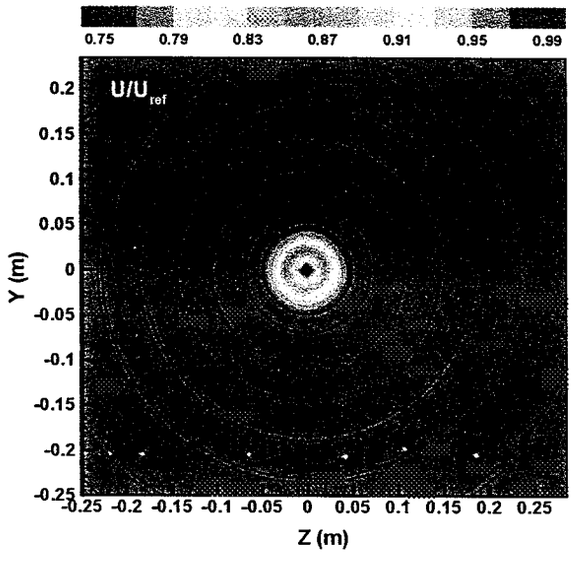

FIGURE 2 – Axial mean velocity map at Station 31, X = 0.469 (m). The white circle marks the initial (inlet) location of the vortex core.

As far as the axial velocity deficit is concerned, we see in this flow that the axial velocity deficit starts by increasing in the beginning of the calculation and then seems to be reaching a maximum where it stabilises. The initial increase of the axial velocity deficit observed in the present study (also reported by Huenecke [5]), must be attributed to "Bernoulli effect" (Batchelor [9]). The stabilisation of the deficit, found in our calculations, should then be followed by a decrease of its value,

according to Ragab and Sreedhar. [10] However, it was not reproduced here due to the relatively small dimensions of the computational domain in streamwise direction.

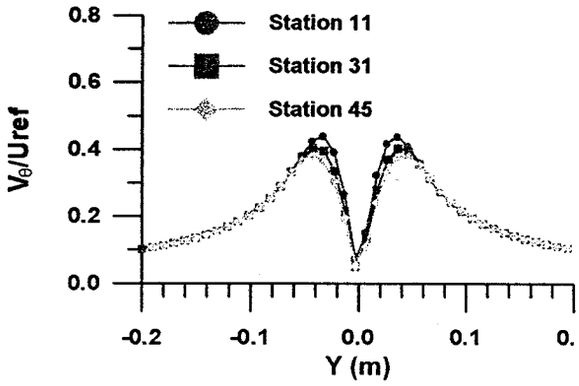

FIGURE 3 – Streamwise evolution of mean tangential velocity profiles through vortex core centres. Stations 11, 31 and 45 correspond to X = 0.080, 0.469 and 0.867 (m), respectively.

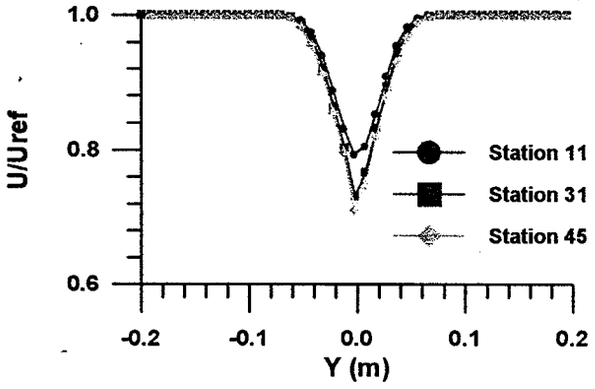

FIGURE 4 – Streamwise evolution of mean axial velocity profiles through vortex core centres. Stations 11, 31 and 45 correspond to X = 0.080, 0.469 and 0.867 (m), respectively.

We now turn ourselves to the understanding of the turbulent field associated with a single vortex. First, the topology of streamwise normal stresses, $\overline{u'^2}$, can be seen in Figures 5 to 7. One may see in Figure 5 that these turbulent stresses reach a peak in a roughly circular region outside the vortex core radius, falling to zero in the vortex core centre and in the outer region. This behaviour is somewhat different from that measured in most experiments in trailing vortices. [11-12] An explanation can be found by noting the fact that our calculations exhibited a negligible amount of meandering, which is in clear contrast with the experimental conditions in the aforementioned investigations. As noted by Green [13], meandering reflects itself in measured data as some kind of small amplitude turbulence and it is present in most wind tunnel measurements. Therefore, the great majority of wind tunnel measurements in trailing vortices exhibits a peak of $\overline{u'^2}$ in their cores, even though as a result of "apparent" turbulence only. The results reported here are, in this way, in very good agreement with the low meandering wind tunnel results of Devenport. [14] Also, this is what one would expect to happen in a single Burgers vortex because there is not any production of turbulence in the vortex core (Zeman [7]). So, any turbulence found there must originate either from the swallowed wake (which we did not consider in our case), or as a result of the interaction with the flow field of another vortex.

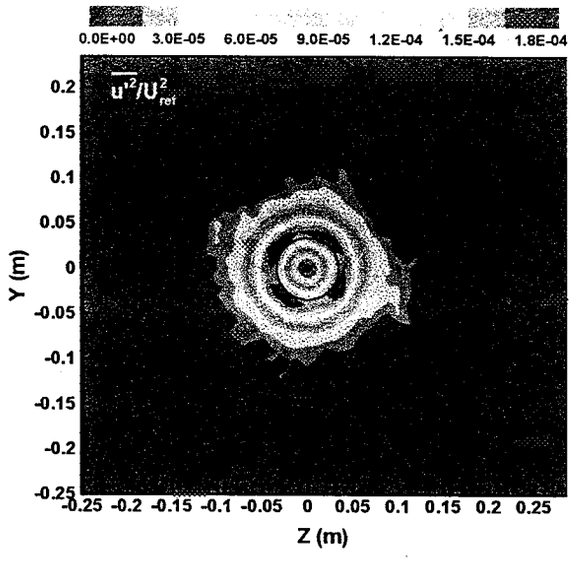

FIGURE 5 – Map of $\overline{u'^2}$ -stresses at Station 11, X = 0.080 (m). The black circle marks the initial (inlet) location of the vortex core.

We also point out here the presence of four large peaks of $\overline{u'^2}$ in the vicinity of the vortex core, which can be seen in Figures 6 and 7 (Station 31). One should note that the aforementioned observation was made in the measured turbulent flow fields reported by Devenport [14] as well. In order to understand its physical origin, one must look first to the results of $\overline{v'^2}$ -stresses. The behaviour of $\overline{w'^2}$ -stresses can then be explained in similar manner.

The presently computed $\overline{v'^2}$ -stresses display approximately the same external contour as those measured by Devenport [14] after filtering (see Figure 8). Unfortunately he does not show much detail regarding how these stresses behave in the vortex cores.

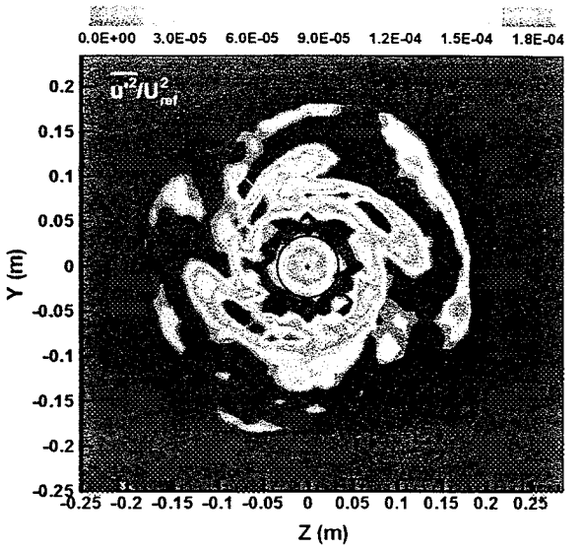

FIGURE 6 – Map of $\overline{u'^2}$ -stresses at Station 31, X = 0.469 (m). The black circle marks the initial (inlet) location of the vortex core.

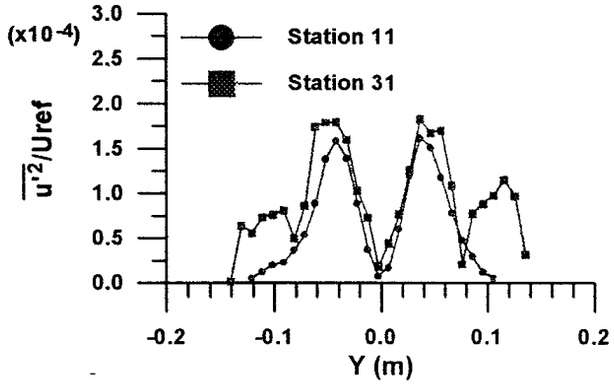

FIGURE 7 – Streamwise evolution of profiles of $\overline{u'^2}$ -stresses through vortex core centres. Stations 11 and 31 correspond to X = 0.080 and 0.469 (m).

One may further observe in Figure 8 that $\overline{v'^2}$ -stresses also exhibit four peaks. The peaks are located precisely in the middle of each one of the four quadrants defined by the system of Cartesian co-ordinates employed in the calculations. At first glance this could be found strange, since one might expect the turbulent fields to be axisymmetric. In fact, a Cartesian representation of field components is probably not the best way to analyse the flow field associated with a single vortex. Observing the SGS contribution to $\overline{v'^2}$ -stresses (not shown), we conclude that their topology coincides with that displayed by the rate of strain tensor (see, e.g., Zeman [7]). This is consistent with the formulation of Smagorinsky's model. However, when we look to the large-scale contribution to these stresses, we see that the same "four peeks" topology found in total (large-scale + SGS) $\overline{v'^2}$ -stresses is present there. This indicates that the so-called "four peeks" topology cannot be attributed to LES modelling. Rather, it has to be explained in terms of large-scale phenomena. In the next paragraph we suggest an explanation to this apparently abnormal behaviour.

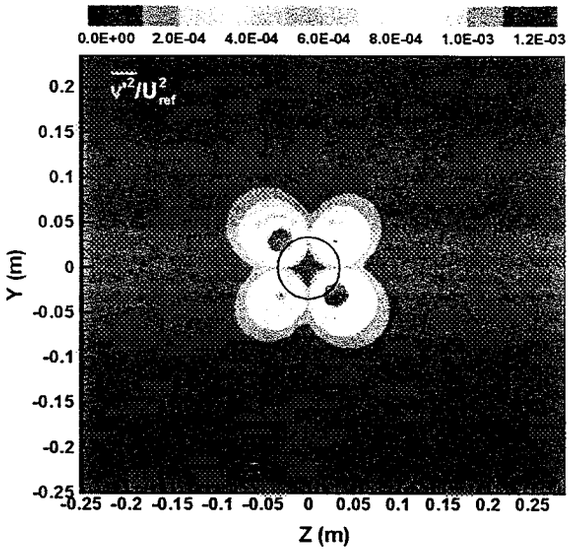

FIGURE 8 – Map of $\overline{v'^2}$ -stresses at Station 11, X = 0.080 (m). The black circle marks the initial (inlet) location of the vortex core.

We see that, although the mean v-velocity reaches its maxima in the (x,y) plane, its highest gradients are located in (x,k) planes, where k is a line making 45 degrees with either y- or z-axis. We also note that $\overline{v'^2}$ is zero in vortex core, at the beginning of our simulations (we do not have entrainment of a wake into the vortex). Thus, it seems natural to conclude that the production term in $\overline{v'^2}$ -transport equation reaches its maximum there, generating the above-referred "four peeks" topology. The same can be said about the $\overline{w'^2}$ -stresses, which exhibit identical topology (except for an already expected 90 degrees rotation). The large levels of $\overline{v'^2}$ - and $\overline{w'^2}$ -stresses (when compared to $\overline{u'^2}$ -stresses) are most likely to be responsible by the energy transfer taking place from $\overline{v'^2}$ - and $\overline{w'^2}$ -equations to $\overline{u'^2}$ transport equation, via pressure-strain term. Hence, this process gives rise to the formation of the "four peeks" also found in $\overline{u'^2}$ -stresses at stations located downstream (see Figure 7).

Observing once again Figures 5 and 6 one can see that, as the vortex evolves downstream,

spiral arms begin to appear. Those arms correspond to the flat "mountains" seen in Figure 7. In this figure one can also find the raising and spreading (by turbulent diffusion) of $\overline{u'^2}$ -stresses in the vicinity of the core region. This phenomenon was found in the LES performed by Ragab and Sreedhar [10] as well, and it is related to the way an unstable vortex reacts to the presence of an initial random perturbation field.

Flap-tip vortex system

In this section we begin the study of the Flap-Tip vortex interaction. It corresponds to the very initial stage of merging of a Flap-Tip vortex pair. As mentioned before, we begin these calculations at an assumed distance, from the wing's trailing edge, of about two and a half wing chords (in reference to the measurements of Huenecke [5]). At such stage, the Flap and Tip vortices have engulfed nearly all the surrounding viscous wake and the flow is then dominated by the dynamics of the interaction between the two vortices.

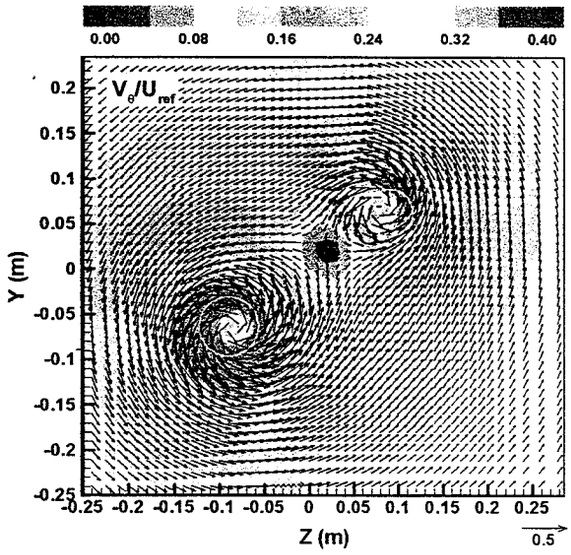

FIGURE 9 – Tangential mean velocity map at Station 13, X = 0.107 (m). The white circles mark the initial (inlet) location of vortex cores.

The first important observation concerns the mean flow topology of the vortices. In fact, the individual vortices loose their original axisymmetry due to reciprocal induction of a strong tangential velocity (defined here as $v_\theta = \left(v^2 + w^2\right)^{1/2}$), which can be seen clearly in the corresponding velocity contours (see Figure 9). The respective tangential velocities increase in the cores as the distance between the two vortex cores becomes larger (it decreases otherwise). This is due to the induced velocity field (Biot-Savart induction) that each vortex imposes to the other. The Flap vortex contains considerably more circulation than the Tip vortex, so it turns out that the latter rotates about the former (see Figure 10). Ultimately, the Flap vortex (larger circulation) will end up by swallowing the Tip vortex. Another aspect of the Flap-Tip vortex interaction, concerning tangential mean fields, can be well appreciated in Figure 11. One may see that the non-axisymmetric tangential velocity fields lead to a slightly larger decay of their tangential velocities and consequent increase of the vortex cores. This must also be due to the fact that Biot-Savart (velocity) induction has augmented the velocities and the velocity gradients near the vortex cores as well.

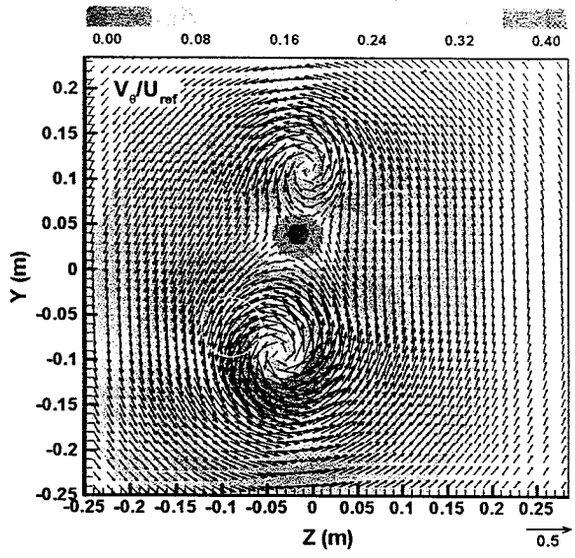

FIGURE 10 – Tangential mean velocity map at Station 55, X = 1.203 (m). The white circles mark the initial (inlet) location of vortex cores.

In the axial velocity contours (Figure 12) we can see that these fields also loose their axissimetry. This result does not result directly from Biot-Savart, which does not play any role in the evolution of axial velocity. Rather, it is a consequence of the rotation of the pair of vortex cores. This also makes the axial fields develop a spiral arm in each one of the vortices. Still more interesting than this observation is what can be seen happening in between the two cores (although not clearly observed in Figure 12 due to the chosen colour map). Figure 13 indicates that Tip and Flap vortices may be in different regimes of the evolution dictated by "Bernoulli effect". The axial velocity deficit in the former vortex is decreasing from the very beginning of our calculation, leading to an interesting phenomenon. It appears that the two vortices exchange some of their axial velocity deficits in the course of their interaction, as a small

axial velocity excess (about 2%) makes a debut in the small space between the pair of vortex cores. Consequently, the axial velocity deficit in the Flap vortex, although still increasing, grows at a much smaller rate than in the single (Flap) vortex case (compare the values of axial velocity for the Flap vortex in Figures 13 and 4). Finally, one should emphasise that both tangential and axial mean fields agree very satisfactorily with those measured by Huenecke. [5] For this purpose we also provide in Figure 14 a perspective view of tangential mean velocity contours in the wake of the aircraft model, showing cut planes where measurements have been carried out.

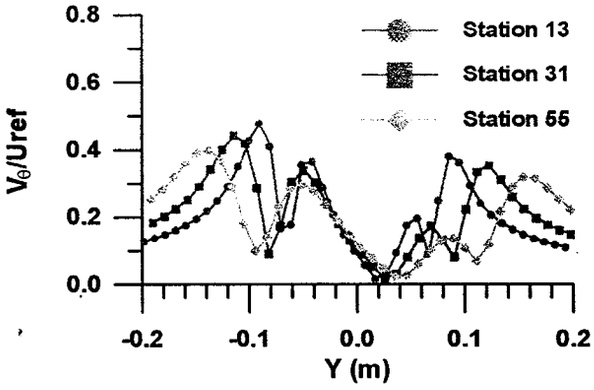

FIGURE 11 – Streamwise evolution of mean tangential velocity profiles through vortex core centres. Stations 13, 31 and 55 correspond to X = 0.107, 0.469 and 1.203 (m), respectively.

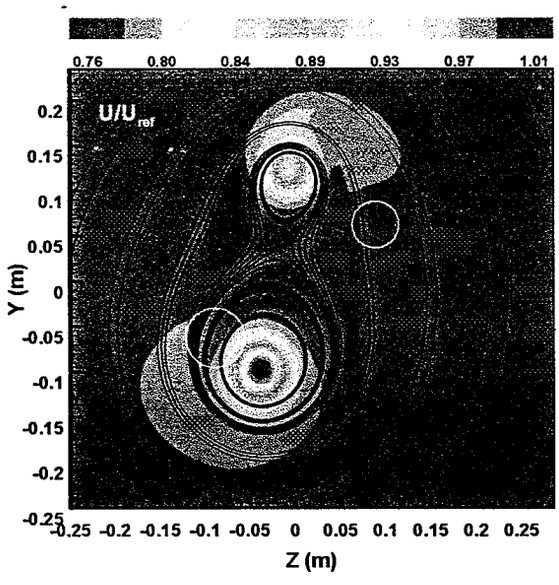

FIGURE 12 – Axial mean velocity map at Station 55, X = 1.203 (m). The white circles mark the initial (inlet) location of vortex cores.

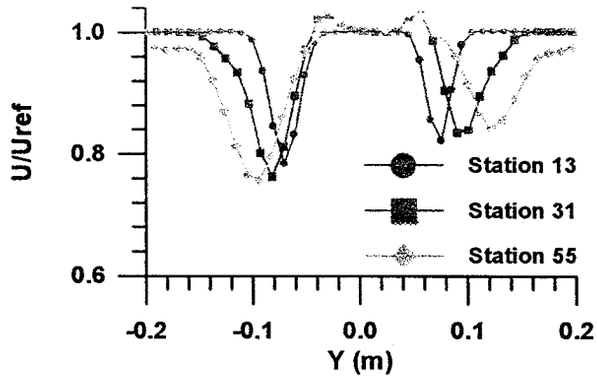

FIGURE 13 – Streamwise evolution of mean axial velocity profiles through vortex core centres. Stations 13, 31 and 55 correspond to X = 0.107, 0.469 and 1.203 (m), respectively.

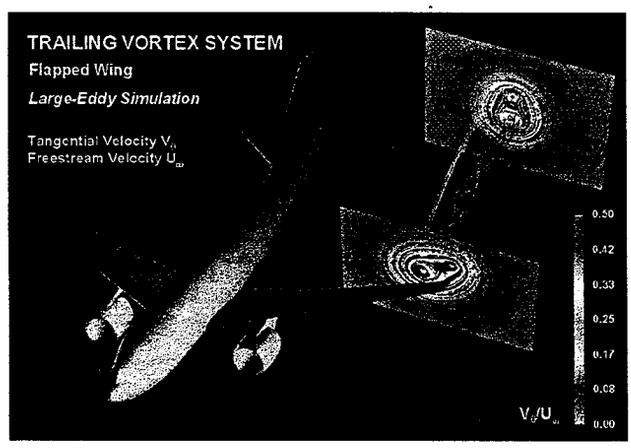

FIGURE 14 – Perspective view of tangential mean velocity contours in the wake of the aircraft model. Calculations start at the third measured plane in the experiments conducted by Huenecke [5] and continue beyond the last of measured planes.

Aiming to analyse the behaviour of turbulent stresses in the Flap-Tip case, we observe Figures 15 to 18. First, it can be seen that the "four peeks" topology (see previous section) is also present in this configuration. The main difference now resides in an increase of the turbulent stresses (both in $\overline{u'^2}$ and $\overline{v'^2}$) occurring in the region of the cores located in between the vortex pair. At first glance, this seems to be in contradiction with the observations made for mean Flap-Tip velocity profiles, which exhibited the opposed behaviour (i.e., tangential velocities increased in the region of the vortex cores that was more distant from the other vortex). However, this apparent discrepancy can be explained if one recalls that the influence of the Flap vortex on the Tip vortex (or vice versa) increases as the distance between them decreases, via Biot-

Savart induction. As a result, the mean velocity variation in a given vortex, due to the presence of another, must be larger in the core region, near the other vortex. So, it turns out that the mean velocity gradient in each one of the vortex cores becomes higher in the same region. The production terms in $\overline{u'^2}$ - and $\overline{v'^2}$ -transport equations are then, once again, responsible for this non-axisymmetric "four peeks" topology.

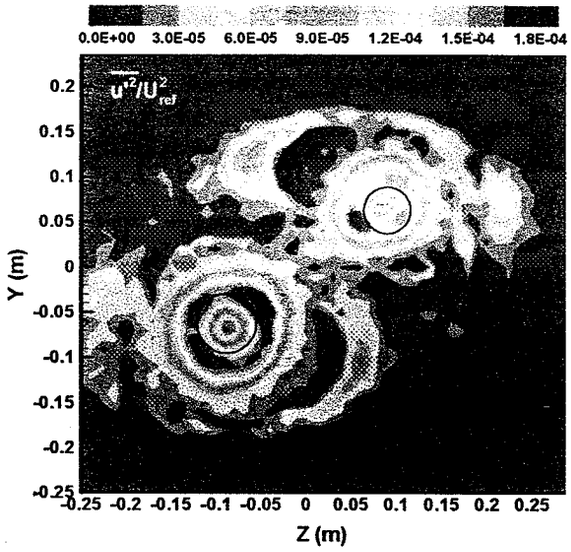

FIGURE 15 – Map of $\overline{u'^2}$ -stresses at Station 13, X = 0.107 (m). The black circles mark the initial (inlet) location of vortex cores.

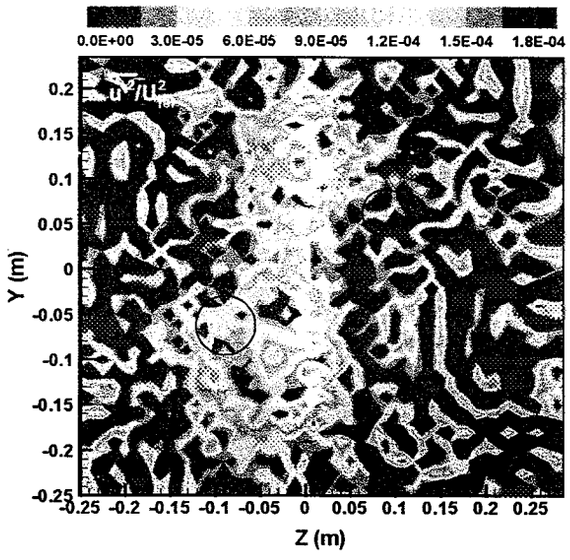

FIGURE 16 – Map of $\overline{u'^2}$ -stresses at Station 55, X = 1.203 (m). The black circles mark the initial (inlet) location of vortex cores.

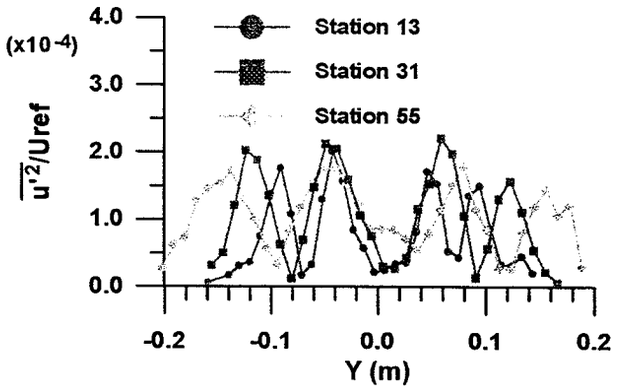

FIGURE 17 – Streamwise evolution of profiles of $\overline{u'^2}$ -stresses through vortex core centres. Stations 13, 31 and 55 correspond to X = 0.107, 0.469 and 1.203 (m), respectively.

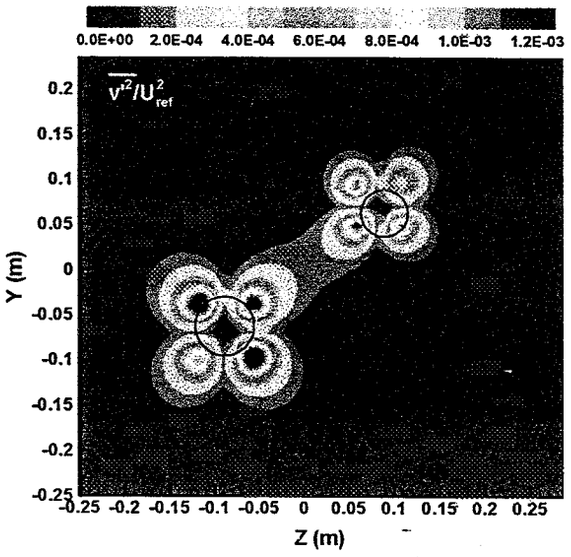

FIGURE 18 – Map of $\overline{v'^2}$ -stresses at Station 13, X = 0.107 (m). The black circles mark the initial (inlet) location of vortex cores.

The above-mentioned increase of turbulent stresses in an interacting Flap-Tip vortex pair is seen more clearly in Figure 17 (compare the peaks of $\overline{u'^2}$ with those in Figure 7). Here, we can also see that there is a process of turbulence exchange between the two vortex cores, portrayed by a growing level of $\overline{u'^2}$ -stresses, as they evolve downstream. This is presumably caused by the outer spiral legs, which happen to be orbiting around each vortex. As the Flap-Tip vortex pair proceeds downstream we observe that, unlike the case of an isolated vortex pair, these legs do not have space to move around the vortices (see Figure 16). Instead,

they fall into a region of very low tangential velocities, located between the pair of interacting vortices. There, the spiral legs seem at first to increase the turbulence level of the flow, establishing some kind of "turbulent bridge" between the two vortices, through which transport of turbulence takes place (see Figures 17 and 18). Nevertheless, the legs are likely to end up by being dissipated because they undergo a process of compression in the aforementioned stagnation point region. Finally, when the roll-up process of the pair reaches completion, all the remaining turbulence from this "turbulent bridge" will be swallowed by the resulting trailing vortex, leading to a further increase in turbulent stresses.

Parametric Study

As we have noticed in the preceding section, the Flap-Tip vortex interaction increases the turbulent stresses in the vicinity of vortex cores. We now argue how this might be used for weakening the circulation of the vortices, relieving the wake hazard problem.

The increase of turbulent stresses in an interacting vortex pair could be used, if properly devised, to augment the turbulence level in the final (rolled-up) trailing vortex issuing from a real aircraft. This would then provide a faster dissipation of the final trailing vortex system. However, there are several possible ways to investigate this hypothesis.

Here we have conducted a first attempt by trying to assess the effect of the initial vortex separating distance in the dissipation of wake vortices. For that propose, we designed the following numerical experiment. We made two LES with the same initial vortex fields as before, but characterised by slightly different initial separating distances between the vortices in the Flap-Tip pair. Those values correspond to variations around the distance set at the beginning of the calculations already discussed in the previous section (d_o = 0.22 m). The results are shown in Table 2. This table shows the evolution of several flow parameters between the start and the end of our computational domain. First, the results concerning the evolution of the circulation $\Gamma(D)$ for all three initial separating distances revealed to be quite disappointing. Although the circulation decreased slightly downstream, only negligible differences were found among the studied test cases. Circulation is known to decrease during vortex merging, [15] but we would expect this reduction to vary with different initial spacing distances. The differences among the values of circulation decay are, peradventure, too small. We acknowledge that our computational domain may be too short to capture such differences. However, we emphasise that the aforementioned differences may be found when simulating the complete process of merging between Flap and Tip vortices. In any case, we find this problem sufficiently interesting to be studied more thoroughly in future investigations.

These calculations still enabled us to find some interesting features concerning the downstream development of the Flap-Tip vortex pair and its dependence upon their initial spacing distance. For instance, in the case of smaller initial spacing, effective merging of the vortex pair was observed. This is illustrated in Figure 19, which shows the map of axial vorticity ω_x in the plane of the vortex cores for d_o = 0.12 (m) at Station 55. However, it can be seen in Table 2 that this fact did not originate any significant change in the evolution of peak vorticity values in the Flap vortex.

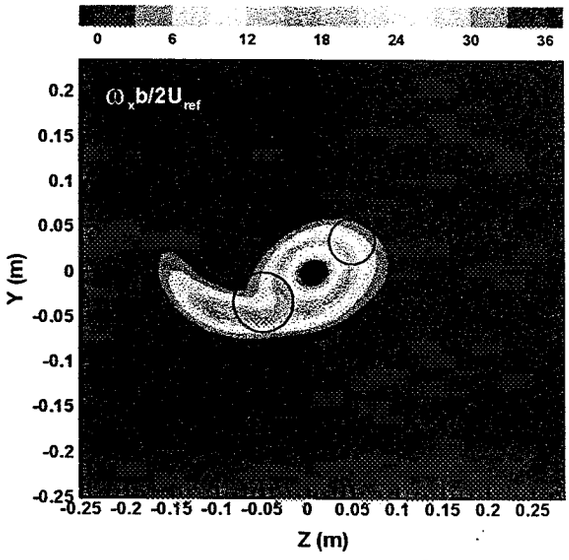

FIGURE 19 – Map of axial vorticity component for d_o = 0.12 (m) at Station 55, X = 1.203 (m). The black circles mark the initial (inlet) location of vortex cores.

As expected by the fact that "Biot-Savart effects" increase with the decrease of spacing distance, the rotation angle θ of the Flap-Tip vortex system displays a strong dependence upon the inverse of the initial spacing. More interesting is to understand the interplay of axial velocity deficits ΔU, between the two vortices. Consistently with our observations about the axial velocity exchange between the cores (slowing each other downstream evolution due to "Bernoulli effect"), we observe that their mutual influence increases if their spacing distance is smaller. The peak values of turbulent kinetic energy k also seem to be reflecting this fact, but only when effective merging occurs.

d_o (m)	0.12	0.22	0.30
Γ_b / Γ_a	0.997	0.997	0.997
θ_b / θ_a	6.847	2.366	1.628
$\{[\Delta U]_b / [\Delta U]_a\}_f$	1.117	1.280	1.322
$\{[\Delta U]_b / [\Delta U_a]\}_t$	0.607	0.896	0.947
$\{[v_\theta]_b / [v_\theta]_a\}_f$	0.806	0.802	0.812
$\{[v_\theta]_b / [v_\theta]_a\}_t$	0.713	0.772	0.786
$\{[\omega_x]_b / [\omega_x]\}_f$	0.648	0.641	0.648
$\{[\omega_x]_b / [\omega_x]_a\}_t$	0.346	0.562	0.606
$\{[k]_b / [k]_a\}_f$	0.451(*)	0.382	0.416
$\{[k]_b / [k]_a\}_t$	–	0.295	0.365

(*) Flap and tip vortices have effectively started merging.
Indices: f = flap; t = tip; a = Station 2; b = Station 55; square brackets denote peak values.

TABLE 2 – Results of the parametric study for the Flap-Tip vortex system.

Conclusions

In this paper, we made several Large-Eddy Simulations in order to understand the physical processes taking place during Flap-Tip vortex interaction. Flap-Tip vortex interaction is known to dominate in the near field established during initial roll-up processes in the wake of aircrafts in high-lift configuration. We have focused on understanding the structure of Flap-Tip vortex turbulent fields and on the mechanisms of interaction. The almost absence of meandering enabled us to cast some light into the behaviour of turbulent stresses (namely $\overline{v'^2}$ -stresses and their interplay with $\overline{u'^2}$ -stresses), that, to the authors knowledge, had never been showed before in any calculations. Finally, we made a first attempt to understand whether the variation of initial spacing distance between Flap and Tip vortices might be used for weakening the circulation of the final rolled-up vortex, ultimately allowing the alleviation of the wake hazard problem.

References:

1. Huenecke, K. (1996) Structure of a transport aircraft-type near field wake. In: *The Characterisation & Modification of Wakes from Lifting Vehicles in Fluids*, AGARD-CP-584.
2. de Bruin, A.C., Hegen, S.H., Rohne, P.B. and Spalart, P. (1996) Flow field survey in the trailing vortex system behind a civil aircraft model at high lift. In: *The Characterisation & Modification of Wakes from Lifting Vehicles in Fluids*, AGARD-CP-584.
3. Pereira, J.C.F. and Sousa, J.M.M. (1993) Finite volume calculations of self-sustained oscillations in a grooved channel. *Journal of Computational Physics*, vol. 106, pp. 19-29.
4. Pereira, J.C.F. and Sousa, J.M.M. (1994) Large eddy simulation of turbulent flow over a cavity. In: *Application of Direct and Large Eddy Simulation to Transition and Turbulence*, AGARD-CP-551.
5. Huenecke, K. (1997) Private communication.
6. Singh, P.I. and Uberoi, M.S. (1976) Experiments on vortex stability. *The Physics of Fluids*, vol. 19, pp. 1858-1863.
7. Zeman, O. (1995) The persistence of trailing vortices. A modeling study. *The Physics of Fluids*, vol. 7, pp. 135-143.
8. Spalart, P. (1998) Airplane trailing vortices. *Annual Review of Fluid Mechanics*, vol. 30, pp. 107-138.
9. Batchelor, G.K. (1964). Axial flow in trailing line vortices. *Journal of Fluid Mechanics*, vol. 20, pp. 645-658.
10. Ragab, S. and Sreedhar, M. (1995) Numerical simulation of vortices with axial velocity deficits. *The Physics of Fluids*, vol. 7, pp. 549-558.
11. Phillips, W.R.C. and Graham, J.A.H. (1984) Reynolds-stress measurements in a turbulent trailing vortex. *Journal of Fluid Mechanics*, vol. 147, pp. 353-371.
12. Wittmer, K.S., Devenport, W.J., Rife, M.C. and Glegg, S.A.L. (1995) Perpendicular blade vortex interaction. *AIAA Journal*, vol. 33, pp. 1667-1674.
13. Green, S.I. (1991) Unsteady flow in trailing vortices. *Journal of Fluid Mechanics*, vol. 227, pp. 107-134.
14. Devenport, W.J., Rife, M.C., Liapis, S.I. and Follin, G.J. (1996) The structure and development of a wing-tip vortex. *Journal of Fluid Mechanics*, vol. 312, pp. 67-106.
15. Shelley, M.J., Meiron, D.I. and Orzag, S.A. (1993) Dynamical aspects of vortex reconnection of perturbed anti-parallel vortex tubes. *Journal of Fluid Mechanics*, vol. 246, pp. 613-652.